JOURNAL OF COASTAL AND HYDRAULIC STRUCTURES

Vol. 5, 2025, 44

Bubble Image Velocimetry application to flow characterization for incipient overtopping events: challenges and opportunities

Corrado Altomare[1], Xuexue Chen[2,6], Alison Raby[5], Xavier Gironella[1], Tomohiro Suzuki[3,4]

Abstract

This study employs the Bubble Image Velocimetry (BIV) technique to characterise the flow velocity of individual extreme waves that overtop sea dikes. Physical experiments were conducted in the small-scale wave flume at the Marine Engineering Laboratory (LIM) of the Universitat Politècnica de Catalunya – BarcelonaTech (UPC). The objective of the experimental campaign was to develop methods to enhance predictive models for wave overtopping volumes of structures with emergent toes. Focused wave groups were used to simulate extreme individual wave overtopping under realistic random sea states. In addition, the campaign prioritized the development of non-intrusive measurement techniques to quantify overtopping volumes and associated flow velocities, leveraging the data gathered throughout the study. To this extent, the present study, in particular, examines the potential of employing the BIV technique for non-intrusive measurements and offers preliminary insights into the characterisation of overtopping flow velocity for the selected structure. The study demonstrates that overtopping flow fields are highly non-uniform, which challenges the assumptions of simplified models such as Boussinesq or non-linear shallow-water models. The BIV technique is therefore crucial in capturing the complex spatial and temporal variations in flow velocities.

Keywords

Wave Overtopping, Flow velocity, Bubble Image Velocimetry, Sea Dikes, Focused Wave Groups, Physical Modelling

[1] corrado.altomare@upc.edu, xavi.gironella@upc.edu, Universitat Politècnica de Catalunya - BarcelonaTech, Spain
[2] TU Delft, Delft, The Netherlands
[3] tomohiro.suzuki@mow.vlaanderen.be, Flanders Hydraulics, Antwerp, Belgium
[4] tomohiro.suzuki@kuleuven.be, KU Leuven, Leuven, Belgium
[5] alison.raby@plymouth.ac.uk, Plymouth University, Plymouth, United Kingdom,
[6] Xuexue.Chen@vanoord.com, Van Oord Dredging and Marine Contractors, The Netherlands

Research Article. **Submitted:** 12 August 2024. **Reviewed:** 22 April 2025. **Accepted** after double-anonymous review: 23 April 2025. **Published:** 19 May 2025.

DOI: 10.59490/jchs.2025.0044

Cite as: Altomare, C., Chen, X., Suzuki, T., Raby, A., & Gironella, X. Bubble Image Velocimetry technique applied to wave overtopping flow characterization - challenges and opportunities. *Journal of Coastal and Hydraulic Structures*. https://doi.org/10.59490/jchs.2025.0044

This paper is part of the **Thematic Series** of selected papers on advances in physical modelling and measurement of Coastal Engineering issues, as presented on the Coastlab Conference in Delft in 2024.

1 Introduction

Understanding the dynamics of extreme wave overtopping is crucial for the design, operation, and maintenance of coastal structures, particularly promenades and waterfronts in urbanized coastal environments. Wave overtopping poses significant risks to infrastructure and public safety, necessitating robust predictive models. This study focusses on methods to characterise the flow velocity of individual extreme waves that overtop promenades in scale hydraulic models using the Bubble Image Velocimetry (BIV) technique, as proposed by Ryu et al. (2005). The primary objective is to enhance the accuracy of models used for forecasting wave overtopping of coastal structures with an emergent toe, commonly found on sandy beaches. Accurate modelling is essential for predicting the impact of extreme wave events and for designing effective coastal defences. For example, Raby et al. (2020) made significant contributions by using high-speed video and BIV techniques to capture wave impacts, enhancing understanding of these complex processes.

The necessity of designing coastal structures to minimize or prevent wave overtopping has long been recognized as essential for ensuring coastal safety. Early research by Endoh and Takahashi (1995) identified the limitations of using a single average flow value or maximum overtopping volume for design, questioning the sufficiency of traditional approaches based on mean overtopping discharges. Schüttrumpf and Oumeraci (2005) published the first study on wave overtopping flow at sea dikes, specifically investigating overtopping layer thickness and velocities, which further highlighted the importance of considering these variables in the design process. Studies by Hughes and Thornton (2016) emphasize that accurately predicting and characterizing significant overtopping events is crucial in certain scenarios. For effective coastal defence design, it is imperative to consider the properties of individual waves, as later confirmed by and Whittaker et al. (2018). Sandoval and Bruce (2017) reinforced these findings by using video evidence from real accidents to assess the dangers of overtopping waves to pedestrians, further underscoring the need for a more detailed understanding of individual overtopping events. Arrighi et al. (2017) standardized the assessment of human stability in floodwaters by accounting for flood characteristics and individual physical attributes. In the same years, Bae et al. (2016) developed criteria to evaluate the stability of individuals exposed to overtopping waves, marking a turning point in research focused on pedestrian safety.

EurOtop (2018) formalized these shifts by establishing guidelines that incorporate both average and maximum overtopping discharge limits, recognizing the difficulties of setting precise thresholds for all conditions. From 2019 onward, research has increasingly focused on the detailed characteristics of overtopping flows. Van Bergeijk et al. (2019) introduced new formulae to describe changes in overtopping flow velocity along dike crests, while Mares-Nasarre et al. (2019) analysed the overtopping layer thickness and velocity on low-crested mound breakwaters, contributing valuable insights into the design of these structures under extreme conditions. Altomare et al. (2020) examined the adequacy of design criteria for coastal defences against wave overtopping, focusing on pedestrian safety on sea dikes. They found that hazards are more accurately assessed by considering the combination of flow velocity and thickness rather than single maximum values (Suzuki et al., 2020). Van der Meer et al. (2022) assessed wave overtopping hazard to pedestrians on coastal structures, presenting new tests that measured flow velocities and thicknesses for stable and unstable conditions. They proposed guidelines to distinguish stable from unstable situations for pedestrians.

In recent years, research has extended into the urban coastal safety domain. Stokes et al. (2021) introduced SWEEP-OWWL, a new forecasting system for predicting wave runup and overtopping volumes along various coastal profiles, significantly improving prediction accuracy and enhancing coastal community preparedness. Most recently, Garzon et al. (2023) proposed the EW-Coast framework to standardize flood warnings and improve prediction accuracy for wave-induced flooding impacts on pedestrians and urban areas.

The assessment of overtopping flow velocity is crucial for evaluating coastal safety and understanding potential risks to pedestrians and vehicles. Numerous studies have proposed formulae to estimate the maximum velocity of overtopping flow at the seaward edge of a dike crest, considering parameters such as wave run-up height and crest freeboard (Schüttrumpf, 2001; Schüttrumpf and Oumeraci, 2005; van der Meer et al., 2010; EurOtop, 2018; Formentin et al., 2019; Mares-Nasarre et al., 2019). Although the existing formulae are commonly applied, they mainly address milder dike slopes, creating a gap in the literature concerning their relevance to steeper dikes. The behaviour of overtopping waves on steeper slopes could vary considerably, emphasizing the need for additional research to confirm or adjust these models for such situations. In addition to these empirical models, measurement techniques for overtopping flow velocity are essential for validating theoretical predictions and improving design safety. Several methods are commonly used to measure flow velocity, each with its own advantages and limitations, as summarized clearly by Koosheh et al. (2021). Mechanical methods, such as micro-propellers, are affordable and simple but require careful calibration to account for factors like submergence, response time, and turbulence. Doppler Effect-based instruments can probably give better estimates of flow velocities in aerated flows, which are common in overtopping events. Remote sensing techniques, such as Particle Image Velocimetry (PIV) and BIV, can measure velocities in aerated regions more effectively.

In the aforementioned context, the present article aims to bridge the gap in understanding the dynamics of individual wave overtopping events by employing advanced techniques such as Bubble Image Velocimetry. The BIV technique is better suited than PIV (Particle Image Velocimetry) for measuring flow velocity in bubbly, aerated environments, such as overtopping scenarios, because it uses naturally occurring bubbles as tracers, avoiding the inaccuracies and optical distortions that can affect PIV in these conditions. Na et al. (2018) investigated large-scale plunging breaking waves and employed BIV to measure surface velocities in the highly aerated regions of the waves. The researchers mounted two high-speed cameras on an instrument bridge, orienting them downward and perpendicular to the still water surface. Utilising commercial software from LaVision, Inc., the researchers processed the images to ascertain the instantaneous velocity fields. The study, which made comparisons between large and small-scale tests, concluded that BIV measurements of flow kinematics in the aerated region, combined with void fraction and turbulence measurements, could be scaled up using the Froude scaling law. The estimated error for the measured mean velocity, calculated using the bootstrap method and normalized by the phase velocity, was 7.2%. Lee et al. (2022) utilised BIV to assess velocities within the aerated regions of bubbly flow on the deck of a rectangular structure, that mimicked a BW Pioneer FPSO (Floating Production Storage and Offloading) during green water events. The authors demonstrated that BIV functions by analysing the texture of the bubble-water interface to determine flow velocities, particularly during the water shipping phase when water moves along the deck. Chuang (2024) investigated flow velocities and patterns in three types of green water events - plunging wave, hammer fist, and plunging dam break, as identified by Greco et al., (2007) - using both PIV and BIV. The study demonstrated the crucial role of BIV in measuring velocities in aerated regions typical of these events.

The present study explores the potential of BIV to improve overtopping predictions and support the assessment of coastal structure performance. This objective will be pursued by focusing on the particular features of overtopping waves. These improvements are crucial for mitigating risks to public safety and infrastructure in coastal areas. To achieve this objective, we conduct detailed analyses of overtopping events, specifically examining the flow velocities of individual waves. By providing a detailed characterization of overtopping flow velocities and validating the BIV technique, this research contributes to the development of more precise predictive models for coastal wave overtopping.

The structure of the present article is outlined here. Introduction: this section introduces the topic of wave overtopping, its significance for coastal structures, and the necessity for accurate predictive models. The study's objectives are delineated, as is the importance of understanding individual wave dynamics in urbanized coastal areas. The methodology employed is described in the Section 2. This section provides a detailed account of the experimental configuration and wave conditions employed in the study. The section goes on to describe the configuration of the small-scale wave flume, the application of the Bubble Image Velocimetry (BIV) technique, and the protocols that were followed during the experiments. The results are presented in Section 3. This section presents the findings of the experimental tests. The key observations and data related to the flow velocities of overtopping waves are highlighted, thereby providing insights into the behaviour of individual waves and their implications for coastal safety. Uncertainties related to the experimental modelling of wave overtopping and the BIV measurements of overtopping flows are described in Section 4. The Discussions and Conclusions in Section 5 considers the implications of the results for coastal engineering and wave overtopping modelling. The findings are interpreted in the context of existing literature and their contribution to a better understanding of wave dynamics and risk assessment is explored. The article concludes with a summary of the principal findings and their significance.

2 Methodology

2.1 Experimental layout and wave conditions

Experimental tests were conducted in the small-scale wave flume (CIEMito) at the Marine Engineering Laboratory (LIM) of the Universitat Politècnica de Catalunya – BarcelonaTech (UPC). The BIV technique was employed for the capture and subsequent analysis of the flow velocities associated with overtopping waves. The utilization of this non-intrusive measurement method enables the comprehensive characterization of wave-induced flows without disrupting the underlying wave dynamics. CIEMito flume is 18 m long and 0.38 m wide. A piston-type wavemaker is employed to generate waves. The CIEMito wave generation does not support wave reflection compensation. However, the utilisation of focused wave groups (see following sections) – which characteristically possess a very short duration – serves to prevent issues related to re-reflected waves at the wave generation that are not absorbed. Consequently, the absence of active wave absorption does not compromise the integrity of the results. A nominally 1:50 scale model was used. The model was made of plywood and comprised a sloping beach composed of a 1:15 slope starting at about 7.2 m from the wave generation and followed by a 1:6.3 slope reaching the toe of the dike/promenade. The use of this steep slope is justified by an analysis of beach profiles from the Maresme region, located in the northern part of Barcelona, Spain. The study reveals the presence of notably steep slopes, particularly in the uppermost sections of the beach within the swash zone.

The structure was designed with different geometries: a vertical wall and sloping dikes with slopes equal to 1:2, 1:1 and 2:1, respectively. In all cases, the height of the dike was 0.04 m. The dike was placed either at the end of the 1:6.3 beach or at a 0.05 m distance, creating a layout with a horizontal emerged berm at the dike toe. A sketch of the wave flume and model layout is depicted in Figure 1. The still water level was lower than the structural toe, resulting in the dikes being exposed: the employed water level was 0.30 m, while the toe of the structure was at 0.324 m above the flume bottom. The crest freeboard was therefore at 0.064 m above the still water level. Eight resistive wave gauges (WG0-WG7) and one ultrasonic proximity sensor (AWG0) were placed along the flume to measure water surface elevation, the distance of which from the wave generator (centre stroke at rest) ranged between 4.00 m (WG0) and 9.58 m (AWG0). An overtopping tank, equipped with a second ultrasonic proximity sensor (AWG1), was used to measure the volume of overtopping.

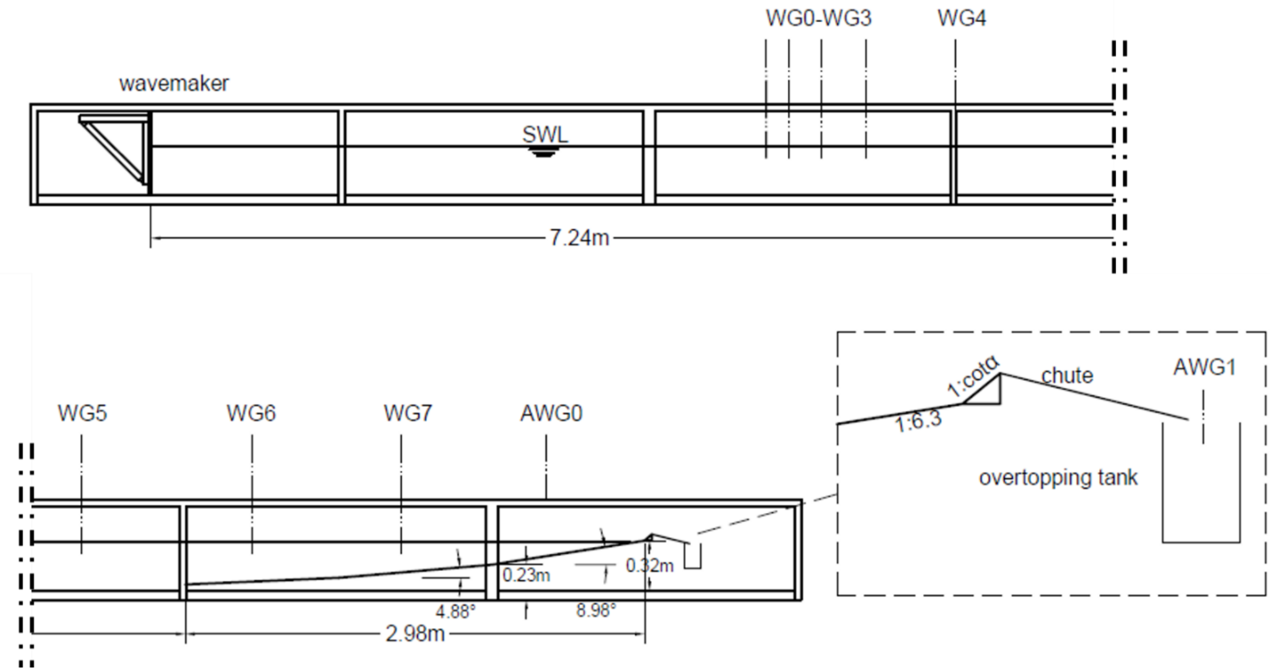

Figure 1: CIEMito 2D lateral view with detail of sea dike and overtopping box.

Hughes and Thornton (2016) and Whittaker et al. (2018) emphasized the importance of considering individual wave properties in the accurate structural design of coastal defences. In order to simulate extreme wave overtopping events, the NewWave theory, as proposed by Tromans et al. (1991), was employed. This theory provides a realistic representation of extreme wave events in a random sea state by correlating the expected shape of a significant wave with the overall characteristics of the sea state. The utilization of focused wave groups, as opposed to long-duration irregular wave time series, offers a number of advantages. The use of focused wave groups enhances the repeatability and accuracy of experimental measurements, as well as the precision of models used to study significant wave interactions (Hofland et al., 2014). Whittaker et al. (2016) demonstrated that focused wave groups are effective for investigating wave-structure interaction (WSI) problems, showing that a single incident group can reproduce extreme coastal responses representative of a given sea state. Accordingly, this study utilized focused wave groups in lieu of random sea states.

The time series for each focused wave group was generated using the NewWave theory, as detailed in Whittaker et al. (2017). This theory describes the most probable shape of a large wave in a given sea state. Originally, NewWave outlined the generation and propagation of a compact wave train on a horizontal bottom. In this study, it was adapted to account for waves shoaling and breaking near a structural location. The focus location is used to control the dispersion of the wave group as it shoals and breaks during propagation. Whittaker et al. (2016) demonstrated that the NewWave theory is applicable in relatively shallow waters (kh<0.5), where linear frequency dispersion remains the dominant mechanism despite increasing nonlinear effects due to bathymetric changes. Theoretically, the energy of the focused wave group is maximized upon reaching the structure if the focus location is sufficiently close. A NewWave-type focused wave group consists of N infinitesimal wave components, defined as follows:

$$\eta(x,t)=\frac{A}{\sigma^2}\sum_{i=1}^{N} S_{\eta\eta}(\omega_i)\cos(k_i(x-x_f)-\omega_i(t-t_f)+\phi)\,\Delta\omega \tag{1}$$

where $S_{\eta\eta}$ is the power spectral density, ω is the angular frequency, t is time, σ is the standard deviation of the sea state, with an associated variance $\sigma^2=\sum S_{\eta\eta}(\omega_i)\Delta\omega$ in this discretized form, and k_i is the wavenumber of the i-th wave component with angular frequency ω_i (related to it by the linear dispersion relation $\omega^2=gk*tanh(kh)$, where g is the acceleration due to gravity and h is the water depth), and x is the horizontal distance. All wave components come into phase at the focus location x_f and focus time t_f to form a large wave with a linear focus amplitude equal to A. A comprehensive range of focusing behaviours can be permitted by incorporating the phase angle ϕ of the group at focus (e.g. crest, trough, …), whereas the energy concentration within the group remains unaffected by the value of ϕ. However, the shape of the wave can influence the patterns of breaking and, consequently, the impact exerted on the structure.

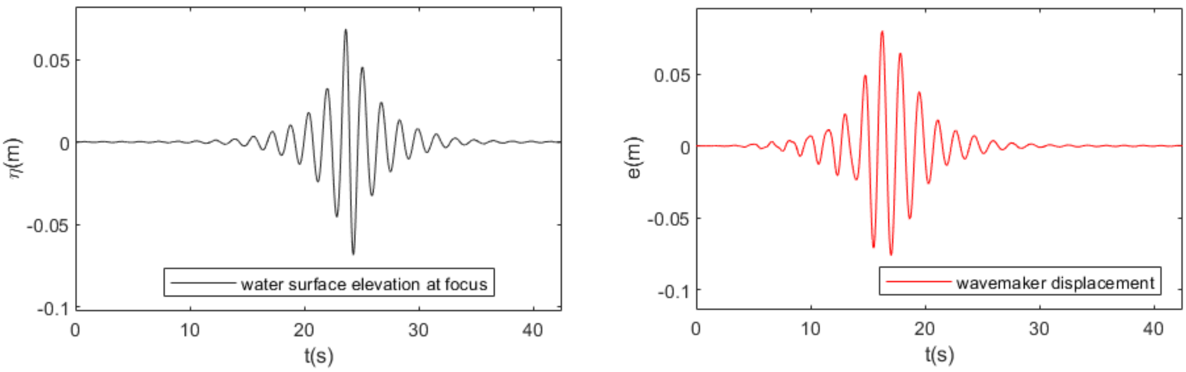

Figure 2: Timeseries of target water surface elevation at the focus location (left) and wavemaker displacement (right) of the tested focused wave group having phase at focus equal to 270°.

For the sake of the methodology development, one focused wave group conditions out of the experimental campaign carried out in the CIEMito flume has been selected. The experiment consisted of focused waves generated starting from the following spectral deep-water wave characteristics: $H_{m0,o}$=0.08 m (focus wave amplitude A≈0.16 m) and T_p=1.6 s.

Focus location was equal to 9.58 m, measured from the wavemaker at rest and corresponding to the AWG0 location, while a 270° focus phase was employed. The timeseries of the target water surface elevation at the focus location and the corresponding wavemaker displacement are depicted in Figure 2. The measured individual overtopping volume associated to this wave conditions ranged between 1.6 and 6 l/m (corresponding to 4000 and 15000 at real scale), depending on the sea dike slope. Snapshot of different individual overtopping events are shown in Figure 3 for the four different dike slopes analysed in the present study.

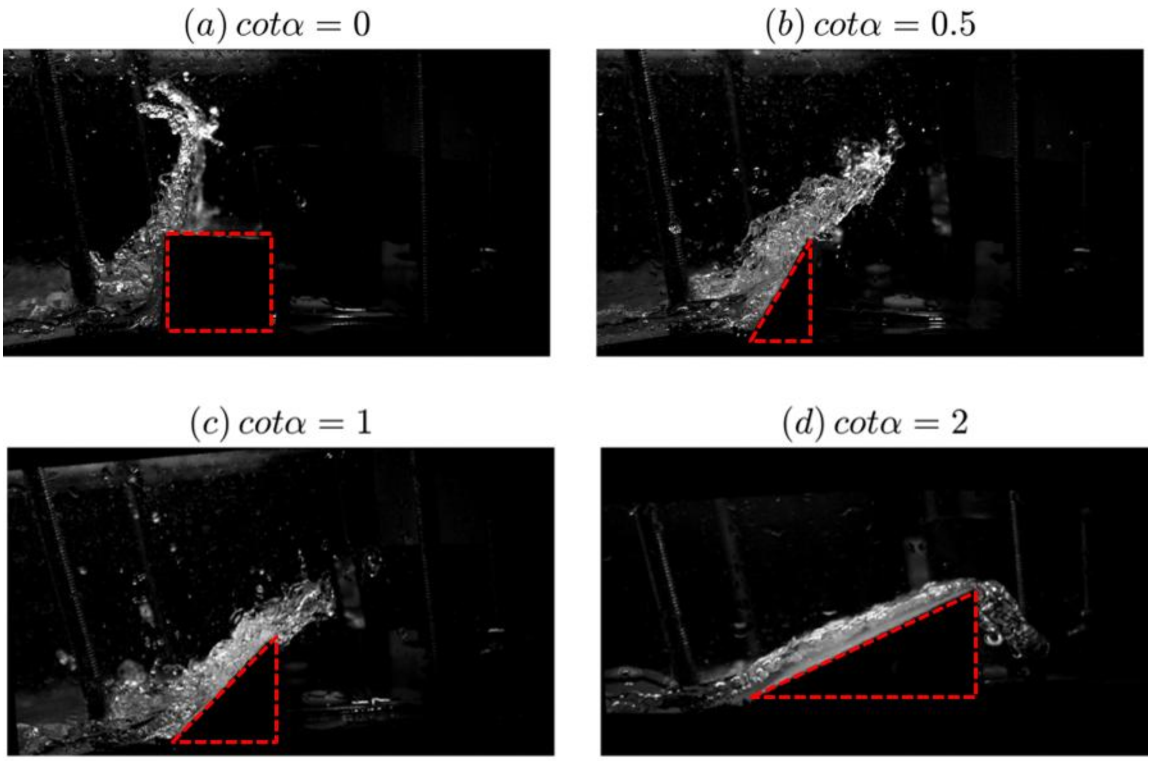

Figure 3: Snapshot of overtopping event on the four sea dike slopes studied here.

2.2 Bubble Image Velocimetry

The BIV method combines the shadowgraph technique, which illuminates the fluid background to show the flow pattern, with the PIV technique, which correlates consecutive images to determine velocity. The shadowgraph technique, in particular, is effective for visualizing non-uniformities in fluids by illuminating the background, thereby revealing the flow pattern. PIV, on the other hand, is a quantitative method that measures the velocity of particles within the fluid, offering precise data on flow dynamics. The velocity is calculated via cross-correlating the images obtained from shadowgraph technique with the bubble structure in the images as tracers. The BIV system normally consist of the following components (Rivillas-Ospina et al, 2012): high speed camera, lights, PIV data processing software, computer for image data process.

The BIV technique is especially suited for environments where PIV might not perform as well, such as in highly aerated or bubbly flow regions, which are common in overtopping scenarios. PIV requires the use of seeding particles that follow the flow, and the technique relies on capturing the movement of these particles to infer the velocity field. In a post wave breaking region, however, the presence of bubbles and turbulence can disrupt the seeding particles' behaviour, leading to inaccuracies in velocity measurement. Moreover, the optical distortions caused by the bubbles can further degrade the quality of PIV images, making it challenging to obtain reliable data. On the other hand, BIV leverages the naturally occurring bubbles as tracers, making it inherently more suitable for bubbly and aerated environments. BIV can capture the velocity of the flow without the need for artificial seeding, thus providing more accurate and reliable measurements in complex flow conditions. This makes BIV a particularly powerful tool for studying overtopping flows, where the presence of bubbles is inevitable.

For BIV, images were recorded using an IDS UI–31800CP–M–GL video–camera with a resolution of 5.1 megapixels (Figure 4). Compromise between sampling frequency and image resolution was achieved by shooting at 118-148 fps. The video camera was located at one side of the wave flume facing the measuring window. The lens was calibrated to focus on a point at a distance from the centre of focal plane equal to 0.97m. Each image was taken with a resolution of 1280x520 pixels. The illumination system consisted of high-power light-emitting diode (LED) lamp built in-house using five lines of high-power LED lamps located on a mobile frame on top of the flume walls. The video images were recorded using the Norpix StreamPix 7 high speed digital recording software.

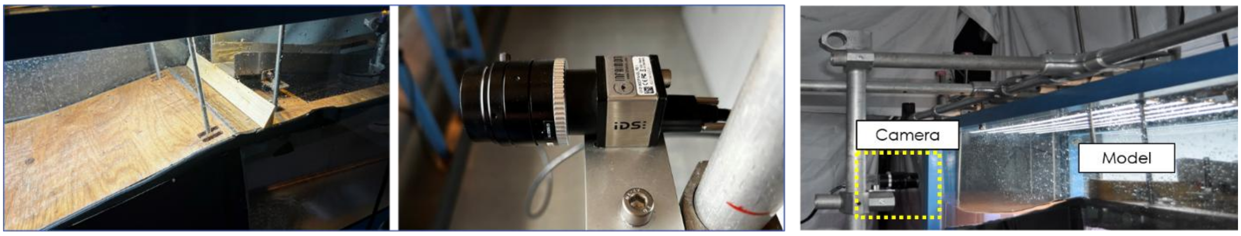

Figure 4: Photos of the 1:6.3 beach and 2:1 dike layout with berm (left) and detail of the IDS UI–31800CP–M–GL video–camera and its installation (centre and right image).

For precise fluid dynamics imaging, careful calibration of the camera system is essential. The camera utilized for capturing images of fluid flow patterns was equipped with a focal length of 55 mm. The circle of confusion, which quantifies the acceptable blur in the image, was determined to be 0.059 mm. The f-number, representing the aperture size of the camera, was set to 2.8. These settings provide a suitable balance between field of view and magnification for detailed visualization of the flow while allowing sufficient light to enhance image clarity. Calibration of the lens was performed to focus on a point at a distance ranging from 0.60 to 0.97 meters from the centre of the focal plane. This range accommodates various experimental configurations, ensuring flexibility in focusing on different regions within the fluid flow setup.

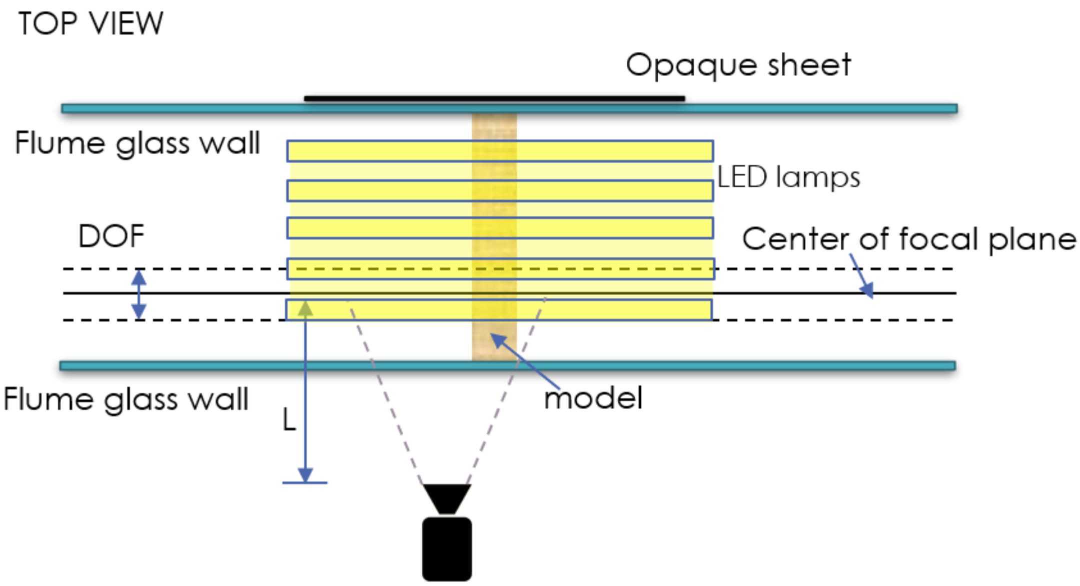

Figure 5: Sketch of the BIV setup (top view).

The depth of field (DOF), indicating the range within which objects appear acceptably sharp, was calculated to be between 2 cm and 5 cm. This narrow DOF ensures that the imaging focuses precisely on the desired plane within the fluid, capturing detailed flow patterns while minimizing background and foreground blur. The relationship between the camera parameters and DOF is given by the formula:

$$DOF = S - R \tag{2}$$

Where,

$$S = \frac{Lf^2}{f^2 + nCL} \tag{3}$$

and

$$R = \frac{Lf^2}{f^2 - nCL} \tag{4}$$

Being f the focal length of the camera focal lens, C the circle of confusion, n the f -number of the camera aperture and L the distance from focal plane (Figure 5). By substituting the aforementioned values of all listed variables into the DOF formula, we derive the range of acceptable sharpness (2 cm to 5 cm), underscoring the need for precise positioning of the focal plane to ensure the region of interest within the fluid remains within the focused depth.

The acquired images underwent meticulous post-processing to enhance the clarity and accuracy of the fluid flow representation. Initially, colours were inverted to obtain a white field with black dots representing bubbles. This inversion facilitates better visualization of flow patterns. The resulting images were analysed using the MATLAB tool The PIVlab (Thielicke & Sonntag, R., 2021). For BIV analysis, the interrogation area was set to 32x32 pixels with a 50% overlap. The velocity field in each interrogation cell was assumed to be uniform. Prior to analysing the full set of frames and generating results, the interrogation cell was carefully selected using an automatic algorithm in PIVlab, which proposes settings based on the image data in the chosen frame. While the evolving nature of the flow along the dike could lead to performance variations between frames, a random check confirmed that the selected settings produced consistent and expected results. Finally, window sizes were refined sequentially to 16x16 pixels and finally to 8x8 pixels, maintaining a 50% overlap. These refinements improve the spatial resolution of the velocity field. A median filter was subsequently applied to the calculated velocity map to eliminate spurious vectors, ensuring a clear and accurate representation of fluid flow dynamics. This step is crucial for reducing noise artefacts and providing a reliable depiction of the velocity field. The temporal evolution of the flow was considered constant over the timescale between image acquisitions. Visual observations indicate no significant changes in the timescale of the phenomenon, at least within the selected frames.

The methodology for BIV analysis comprises a series of essential stages, each of which is designed to guarantee the precision and dependability of the measurements obtained with regard to fluid flow dynamics. The initial step is to delineate the region of interest (ROI) within the captured images. This process concentrates the analysis on the pertinent section of the image, thereby enhancing computational efficiency and ensuring that the measurements are directly applicable to the area of interest. Next, a mask is applied to the ROI to pre-process the images. This step involves several sub-processes:

- Morphological Filtering: using morphological operations to enhance the features of interest in the image, such as particles or bubbles representing the fluid flow. These operations can help in reducing noise and improving the clarity of the features.
- Mask Application: to apply the processed mask to the ROI to isolate the features of interest from the rest of the image. This step ensures that only the relevant data is used for further analysis.

Snapshot of the main post-processing stages to attain the reconstruction of the velocity vector field are depicted in Figure 6.

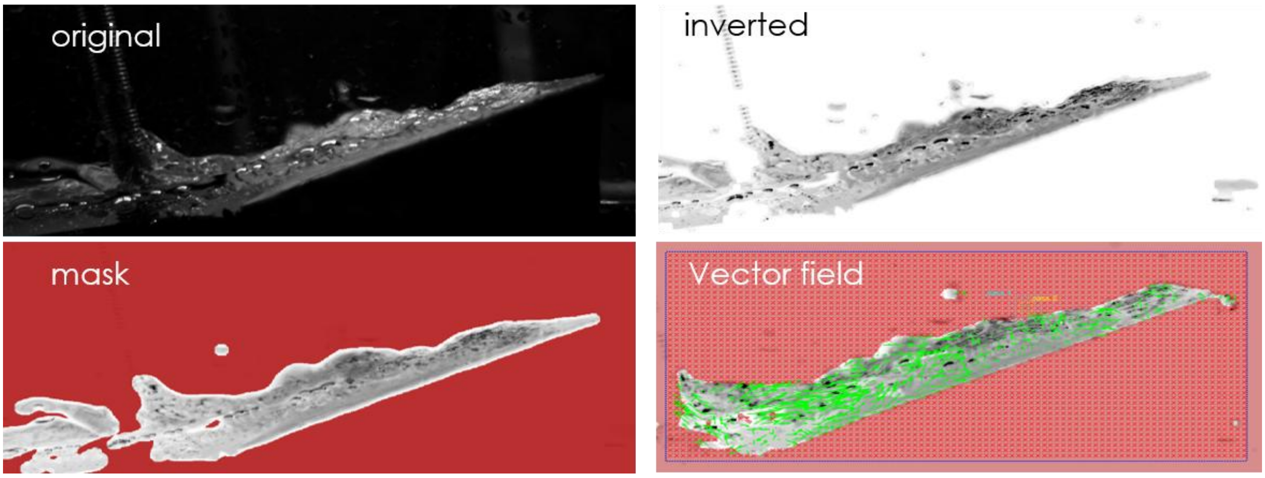

Figure 6: Snapshot of the post-processing steps from the original picture to the reconstruction of the vector field.

After masking, calibration is applied, using a reference image to properly convert pixels to meters and assign the image framing rate in order to define the temporal scale to determine the flow velocity. Then, cross-correlation is used to calculate the displacement of flow features by comparing two consecutive images. Instead of tracking individual particles, cross-correlation identifies the most probable displacement of intensity patterns (regions of similar flow features) between frames. The displacement is determined by locating the peak in the correlation matrix, which represents the most likely shift of flow patterns, allowing for the estimation of velocity fields (Thielicke & Stamhuis, 2014). Finally, perform vector validation to ensure the accuracy of the detected flow vectors. This involves two main filtering steps:

- Standard Deviation Filter (stdf): to apply a standard deviation filter to the velocity vectors to remove any spurious vectors that deviate significantly from the mean. In the present study, velocities that are outside the mean velocity ± 8 times the standard deviation are removed. The value of 8 corresponds the default values suggested by the PIVlab developers. The stdf helps in identifying and eliminating outliers, ensuring that the remaining vectors are representative of the actual flow.
- Local Median Filter (Lmf): to use a local median filter to smooth the velocity field and further remove any remaining outliers. This filter replaces each vector with the median value of its neighbouring vectors, providing a robust measure that is less sensitive to outliers. The Lmf discards vectors if the difference is above the selected threshold. The latter is defined as three times the median value of the residuals (Westerweel and Scarano, 2005), which are calculated as the absolute values of the differences between the individual vector velocity and the median of the neighbour vectors.

The validity of the detected vectors is then assessed based on Valid Detection Probability (VDP) and two criteria:

- VDP (stdf): to ensure that the valid detection probability is greater than 70% when using the standard deviation filter. This means that at least 70% of the vectors should pass the standard deviation filter validation, indicating a high level of confidence in the accuracy of the detected vectors.
- VDP (Lmf): to ensure that the valid detection probability is greater than 50% when using the local median filter. This threshold indicates that at least half of the vectors should pass the local median filter validation, providing additional confidence in the reliability of the velocity field.

By following this methodology, it is possible to obtain a clear and accurate representation of the fluid flow dynamics within the region of interest. The integrated application of morphological filtering, image binarization, vector validation and filtering techniques guarantees the reliability and significance of the BIV analysis, which is vital for the comprehension and modelling of fluid flow behaviour.

2.3 Uncertainty estimation

To assess the accuracy and reliability of overtopping flow velocity measurements, the Coefficient of Variation (CoV) has been employed: the CoV, a normalized measure of dispersion relative to the mean, enables effective quantification of measurement variability. In this study, the CoV is applied to overtopping flow velocities by conducting 20 identical tests under controlled conditions. Each test measured the velocities at the onset of the overtopping process near the dike crest, a critical point where flow characteristics significantly impact the assessment of coastal defence performance. By maintaining consistent conditions across tests, such as wave height and flow rate, the experiment ensured that the variability observed in the measurements was solely due to inherent measurement error rather than external factors.

During each test, velocities were analysed by means of BIV technique as above described: the value of velocity at the beginning of the overtopping event at the dike crest was measured for each of the 20 repetitions of the same testcase and same dike layout. The mean velocity for each set of 20 repetition was then calculated. This mean velocity serves as a reference for evaluating measurement consistency. The standard deviation of the velocities across the 20 tests for each dike layout was then computed to reflect the degree of variation from the mean.

The CoV was calculated using the formula:

$$\mathrm{CoV} = \frac{\sigma'}{\mu} \times 100\ \% \tag{5}$$

where σ' represents the standard deviation of the velocities, and μ is the mean velocity. This percentage-based measure provides a normalized view of variability. The resulting CoV quantifies the relative variability of the overtopping flow velocities. A lower CoV indicates that the measurements are consistent and accurate relative to the mean, suggesting high precision in the measurement process. Conversely, a higher CoV points to greater variability, which could indicate potential sources of error or inconsistencies in the measurement approach.

3 Results

3.1 Overtopping flow velocities

As already mentioned above, irregular wave height, $H_{m0,o}$=0.08 m, and peak period, T_p= 1.6 s, along with focused location x=9.58 m and phase equal to 270° were employed to generate the focused wave group, which was repeated 20 times per structure, so that accuracy of the analysis (mean error and standard deviation) and repeatability were checked. Using an in-house MATLAB script, the acquired images were treated: colour was inverted to obtain white field and black dots (=bubbles), and contours of the flow were identified in order to apply a mask to each picture and remove possible background noise for further analysis. Finally, the PIVlab MATLAB tool was employed to analyses all frames and characterize the flow velocity, following the methodology described in Section 2.2. Finally, BIV has been validated using a Manual Bubble Tracking (MBT) technique as the one described in Raby et al. (2019): details are reported in section 3.2.

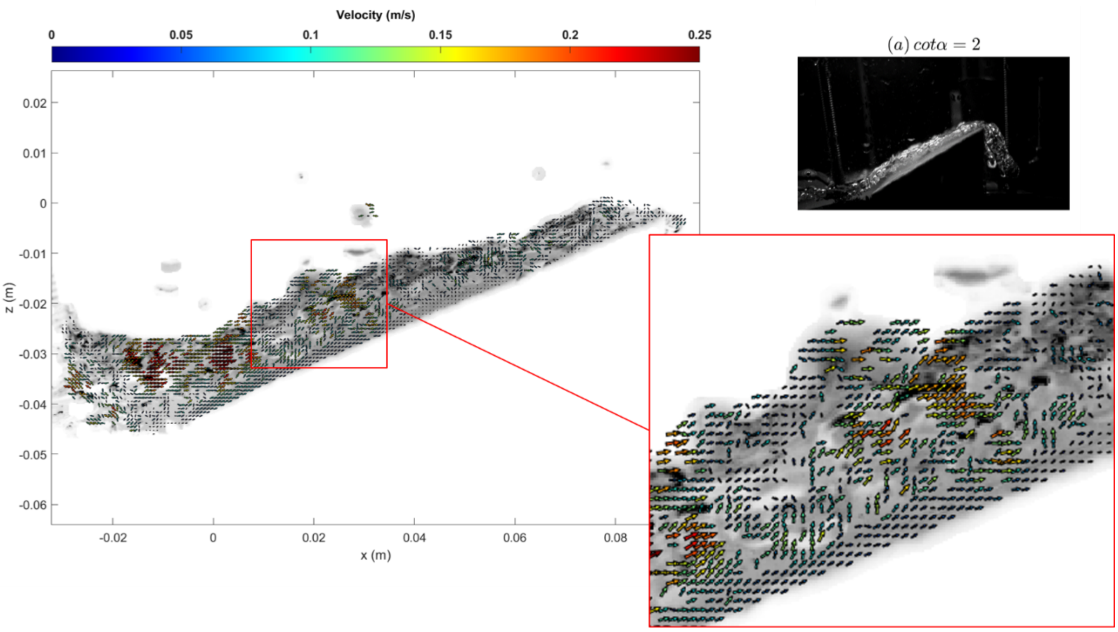

Figure 7: Reconstructed velocity field of the 1:2 dike slope, at incipient overtopping.

The reconstructed velocity field is illustrated in Figure 7, specifically capturing the onset of overtopping on a dike with a 1:2 slope. The figure displays velocity vectors, represented by arrows, with a detailed view provided in an inset box on the right-hand side. The coordinate system of the picture is established such that the origin is positioned at the dike toe. The velocity distribution is color-coded as indicated by the accompanying colour bar, with observed velocities reaching up to 0.29 m/s, which at 1:50 scale might correspond to prototype velocities of 2.10 m/s. An analysis of the vector field reveals a predominant upward and landward net transport throughout the water column. Additionally, the presence of both clockwise and counter clockwise eddy structures is noted, though these features are expected to become more pronounced with steeper dike slopes.

Further results for the other three dike slope configurations are presented in Figure 8. Notably, these configurations exhibit higher maximum velocity values compared to the 1:2 slope, particularly evident in the case of the vertical wall. In this scenario, the velocity vectors predominantly point upward, indicating a significant alteration in flow momentum upon impact with the wall. However, the peak velocity in this configuration is not associated with the up-rushing flow but rather with the horizontal velocity component just prior to the flow's impact on the wall. The flow near the vertical wall also exhibits more complex turbulent structures when compared to those observed near sloping dikes. For the 1:1 slope, a notable horizontal component of the velocity field is observed, not only at the crest edge but also in the region immediately preceding it. Conversely, the velocity field for the 2:1 slope appears to be dominated by a predominantly vertical component.

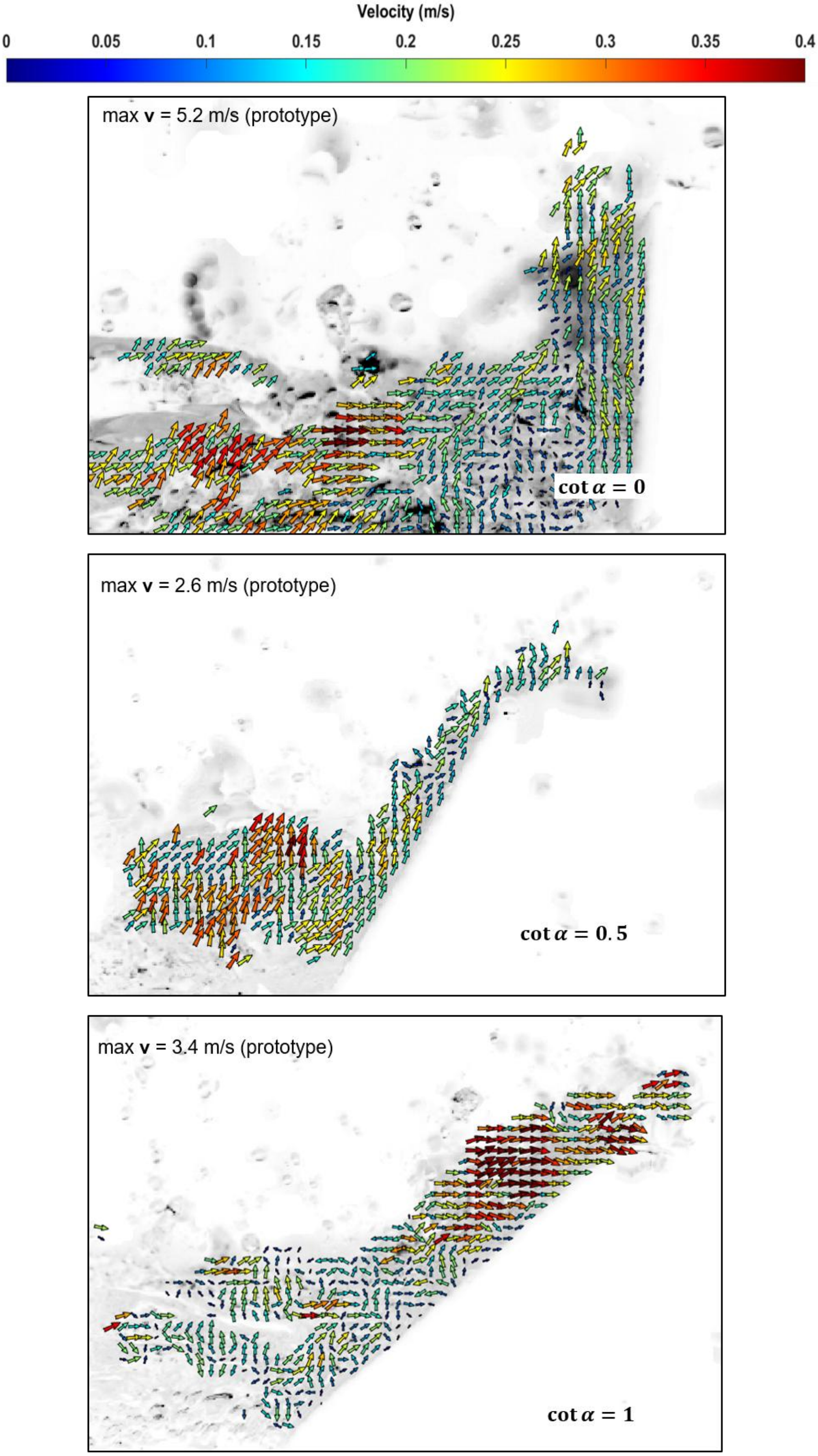

Figure 8: Reconstructed velocity field of the 1:2 dike slope, at incipient overtopping.

While a single focused wave group was selected out of the conducted experimental campaign for the BIV application, the use of four distinct dike slopes allowed evaluating the reproducibility of the BIV technique under varying wave-structure interaction scenarios. This demonstrated the applicability of the BIV technique to processes that, despite being generated by the same wave group, differed due to the influence of slope-induced turbulence and flow characteristics. Results of the coefficient of variation and valid detection probability of each dike slope are presented in Table 1. It should be noted that the coefficient of variation (CoV) is calculated based on the data from one frame, which corresponds to the onset of overtopping, and is derived from the results of the 20 repeated tests. The CoV is notably low for the 1:2 slope, demonstrating an increase for steeper slopes. This indicates that the 1:2 slope exhibits greater reproducibility. It is anticipated that this is attributable to the turbulence inherent to each case; greater turbulence results in decreased repeatability. Although turbulence may present a challenge in terms of test repeatability, it offers a distinct advantage in post-processing the acquired images and validating the detected vectors. Indeed, the VDP increases in line with the slope. For slopes of 1:1 or greater, the VDP is almost equal to 1 when the standard deviation filter is used. Conversely, lower values of VDP are calculated when the local median filter is employed, which is a more restrictive criterion for error estimation.

Table 1: Values of CoV and VDP for BIV velocity measurement of each dike slope.

Dike slope	CoV [%]	VDP (stdf) [%]	VDP (Lmf) [%]
1:2	1.8	70.3	56.7
1:1	3.0	97.1	61.0
2:1	6.6	99.0	57.9
Vertical	3.1	99.8	66.5

3.2 BIV validation

3.2.1 Manual Bubble Tracking

BIV results were validated using Manual Bubble Tracking (MBT), following a methodology similar to that described in Raby et al. (2019). MBT involves determining the position of bubbles in two consecutive frames. A custom MATLAB script was developed to manually select bubbles, to store the position they have in both frames, and to convert pixel coordinates to metres. The distance travelled by the bubbles was then calculated, from which the bubble velocity was determined. The final bubble positions in the second frame were employed to define interrogation areas of 32x32 pixels, the coordinates of which were exported to a .mat file for subsequent import into PIVlab.

PIVlab allows the extraction of velocity values at selected areas. Velocity measured by PIVLab with BIV (v_{BIV}) was finally compared with the manually calculated velocity (v_{MBT}). It is important to acknowledge that the MBT method is subject to some operator judgement, especially when determining the precise location of individual bubbles. In order to reduce this error, the manual selection of the location of each selected bubble per frame has been repeated three times.

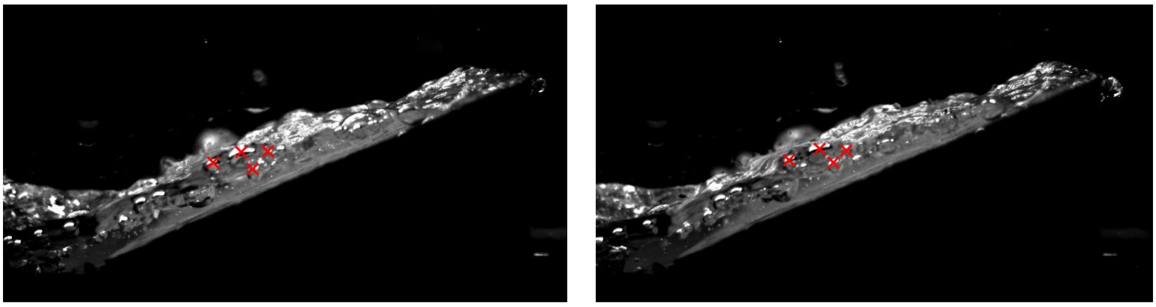

Figure 9: Position of the selected bubbles (red crosses) for MBT in frames 34 (left) and 35 (right).

The MBT analysis reported here pertains to the case of the 1:2 dike slope. In order to ensure consistency with previously reported results (see Section 3.1), the analysis has been concentrated first on the instant of incipient overtopping (corresponding frames 34-35 of the acquired images). Moreover, a subsequent phase of the overtopping process, characterised by higher velocities and more turbulent fields, has been analysed to ensure comprehensive assessment of the validation process (corresponding frames 37-38 of the acquired images).

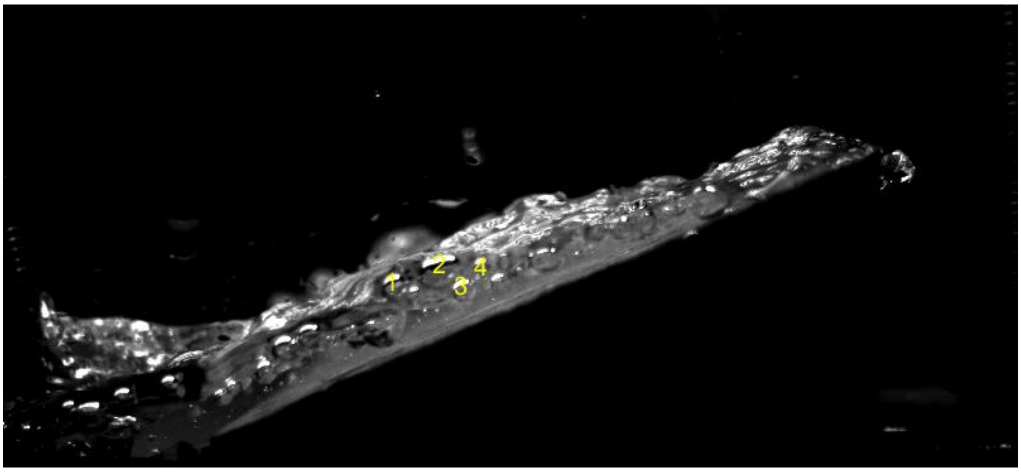

Figure 10: Bubbles number in frame 35.

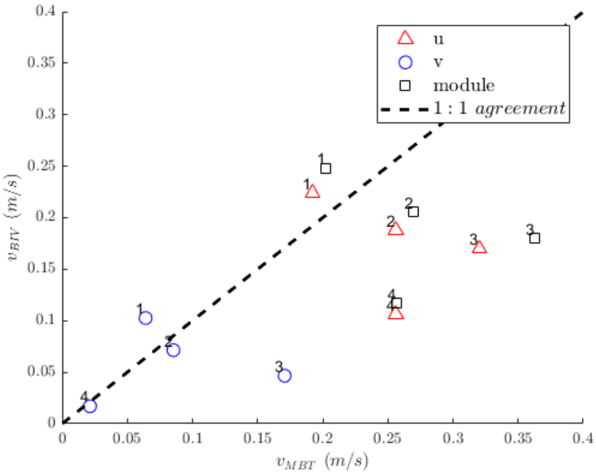

Figure 11: Frames 34-35, comparison of velocity estimate with MBT and BIV for the instant corresponding to incipient overtopping: horizontal component of velocity (triangle); vertical component of velocity (circle); velocity module (square).

Four bubbles identified for both pair of frames are shown, marked by red crosses in Figure 9 and Figure 12. Bubbles are numbered from 1 to 4, as indicated in Figure 10 and Figure 13. The comparison between MBT and BIV results is shown in Figure 11 and Figure 14. For both cases, the Mean Absolute Error (MAE), the robust Coefficient of Determination (R^2) – applied through the utilisation of the *robustfit* MATLAB function -, and the Concordance Correlation Coefficient (CCC) have been employed to estimate the error between the MBT and BIV measurements. The use of robust R^2 allows for a better handling of outliers, providing a more accurate measure of model fit when the data exhibits large scatter (Huber, 1964; Renaud and Victoria-Feser, 2010). Similarly, the CCC offers a comprehensive measure of agreement, combining both precision and accuracy, which is particularly useful for assessing the degree to which two variables agree beyond just correlation (Lin, 1989). In the case of incipient overtopping, the data exhibit significant scatter, particularly due to the estimation of the velocities of bubbles 3 and 4, which are closer to the dike surface and further from the free surface. MBT consistently shows higher velocities than BIV, likely due to measurement or model limitations. In contrast, the agreement for bubbles 1 and 2 is more acceptable, with good correspondence for both velocity components and the resultant velocity module. The calculated MAE is 0.084 m/s, indicating low overall accuracy, as reflected by the CCC = 0.45 and Robust R^2 = 0.4. These values suggest a moderate degree of agreement but highlight the impact of large scatter and measurement uncertainties on the error metrics. For the second set of frames analysed, where the process is slightly more turbulent and involves a greater number of bubbles, the agreement improves significantly. This is visually confirmed in Figure 14, where the MAE reduces to 0.031 m/s, and both CCC and Robust R^2 improve to CCC = 0.78 and Robust R^2= 0.77. These values reflect a much better correlation and a more reliable fit of the data, suggesting that the turbulence and bubble dynamics in this later stage of the process lead to more consistent velocity measurements.

Finally, it is important to note that BIV provides average velocities over interrogation areas (see Section 2.2), whereas MBT tracks individual bubbles. Considering the results presented, it is clear that the process on the 1:2 dike is particularly challenging for both methods, as it involves complex flow dynamics that are difficult to capture accurately. Discrepancies between the velocities obtained from BIV and MBT are to be expected due to the inherent differences in each technique. However, the reader must consider that the comparison has been carried out for the most challenging case in terms of flows features, i.e. the one with less turbulent flow. As outlined in Section 3.1, whilst turbulence can engender challenges with regard to the reproducibility of tests, it concomitantly offers a distinct advantage for the post-processing of acquired images and the validation of detected vectors (as demonstrated by increased values of VDP). The gentlest dike has shown the lowest VDP values. Thus, it is to be expected that there will be larger scatters and greater inaccuracies in the application of MBT and in the comparison with BIV. Notwithstanding it, the comparison demonstrates a reasonable degree of agreement, confirming the reliability of BIV for estimating bubble velocities and, consequently, flow velocities in the regions of interest. As also underlined by Raby et al. (2019), the results indicate that BIV can accurately predict bubble velocities, particularly in areas of strong flow where the bubble velocities closely match the flow velocity.

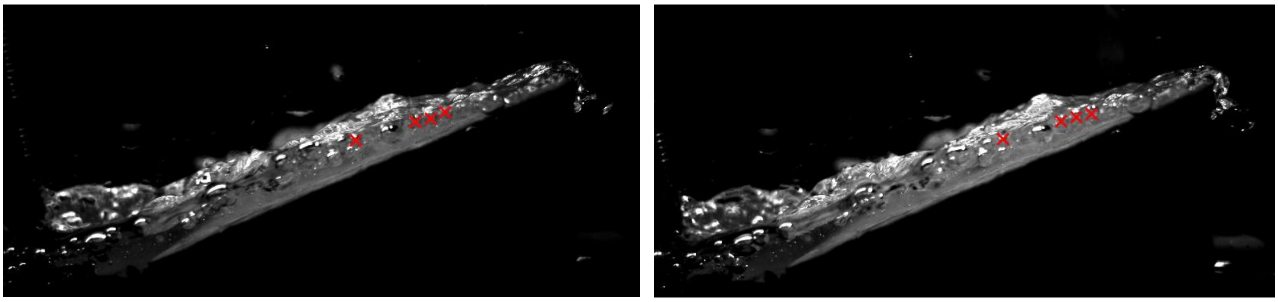

Figure 12: Position of the selected bubbles (red crosses) for MBT in frames 37 (left) and 38 (right).

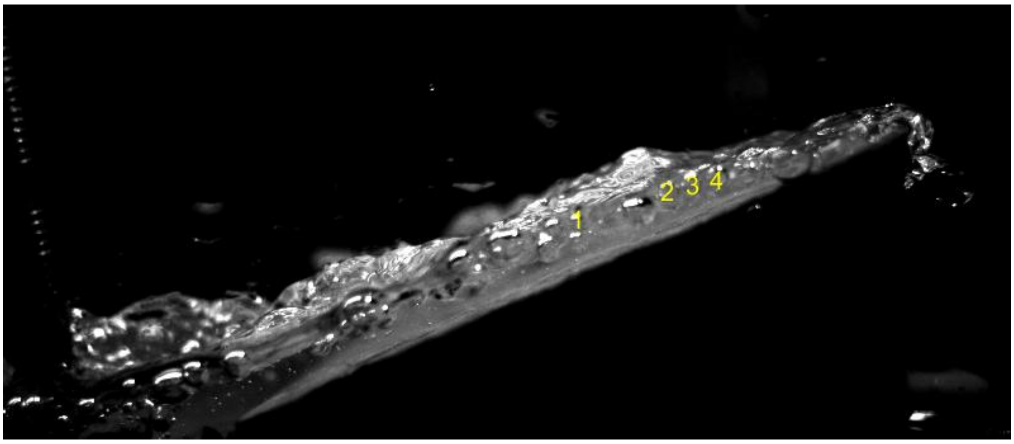

Figure 13: Bubbles numbers in frame 38.

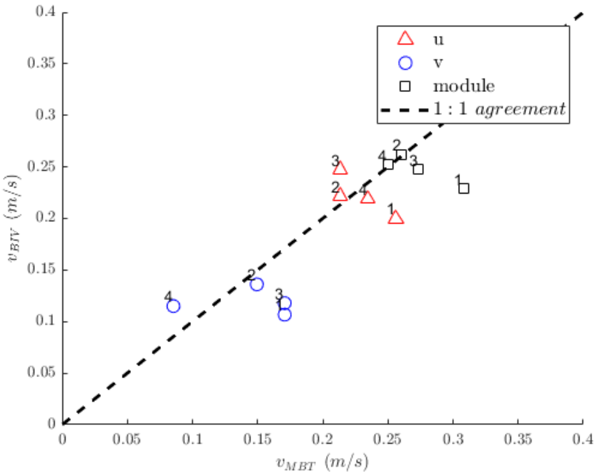

Figure 14: Frames 37-38, comparison of velocity estimate with MBT and BIV: horizontal component of velocity (triangle); vertical component of velocity (circle); velocity module (square).

3.2.2 Bubbles trajectory

To compare BIV with other techniques such as MBT, it is important to highlight that while the robustness and accuracy of the proposed analysis can be justified, this alone does not guarantee that the bubble velocity corresponds precisely to the actual flow velocity. In the absence of redundant measurements or techniques during the experimental campaign, an analysis of the bubble trajectory was conducted to ensure that the bubbles followed the flow accurately. This analysis entailed tracking the movement of the bubbles and comparing their trajectories with the expected flow patterns. By observing the movement of the bubbles, particularly their rise in low-velocity regions, it was possible to assess whether buoyancy was influencing the measurements. This process helps confirm that the bubbles behave as passive tracers or identifies where deviations may occur due to buoyancy effects.

The results of this analysis are here presented. A bubble of relatively large size (so more prone to buoyancy) has been selected as tracer for this analysis. A series of 30 frames have been analysed. For the selected bubble, the displacements and velocities over time have been assessed. The trajectory of the selected bubble is reported in Figure 15, Figure 16 and Figure 17, superimposed to on the first, intermediate and last frame, respectively. The intermediate frame is here considered as the frame corresponding to the incipient overtopping.

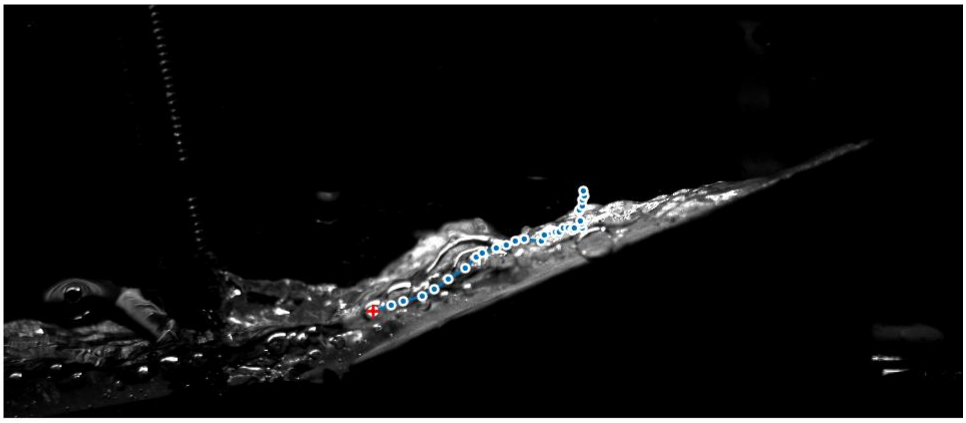

Figure 15: Trajectory of the selected bubble over 30 frames (white circle along blue line), superimposed on the first frame. The bubble position corresponing to the selected frame is marked with a red cross.

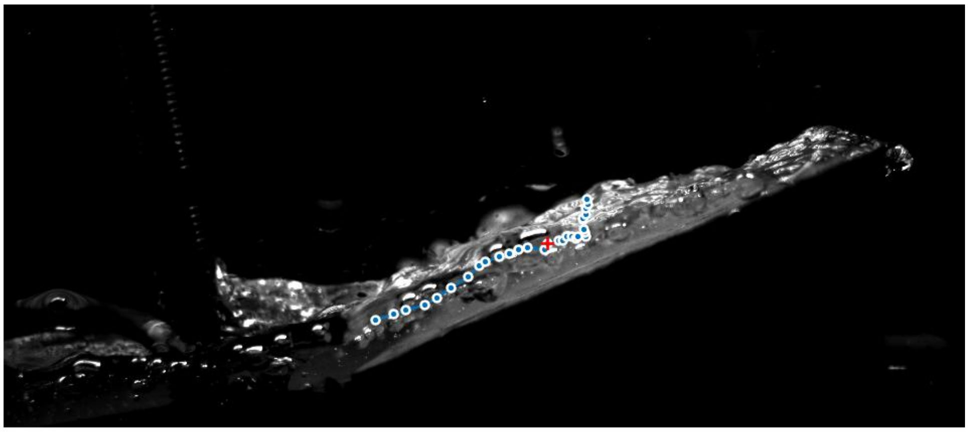

Figure 16: Trajectory of the selected bubble over 30 frames (white circle along blue line), superimposed on the frame corresponding to incipient overtopping. The bubble position corresponing to the selected frame is marked with a red cross.

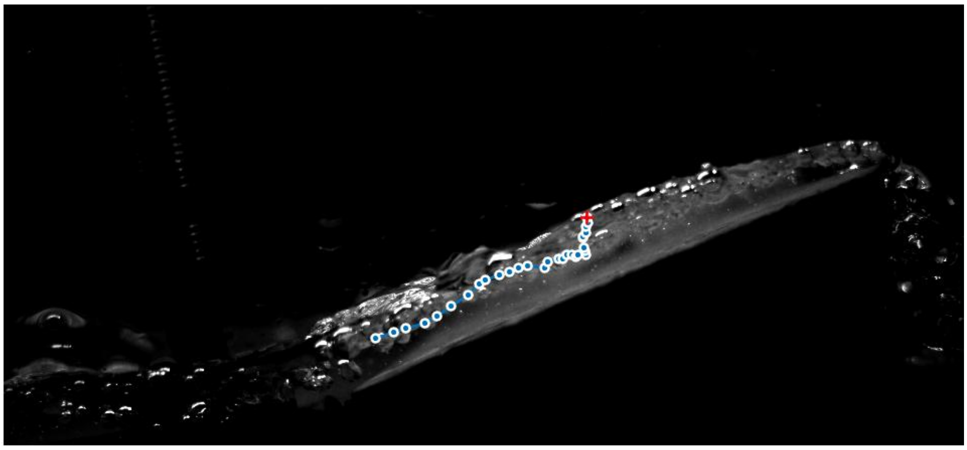

Figure 17: Trajectory of the selected bubble over 30 frames (white circle along blue line), superimposed on the last frame. The bubble position corresponing to the selected frame is marked with a red cross.

As demonstrated in Figure 18, the velocity of the bubble, both in magnitude and for each component, undergoes an evolution. A thorough examination of Figure 18 and the bubble trajectory previously outlined reveals that for the majority of the run-up and overtopping process, the bubble follows the flow path almost parallel the dike slope. However, a notable deviation occurs when the horizontal velocity undergoes a substantial decrease. In such instances, the bubble initiates a process of ascent towards the free surface, characterised by minimal horizontal displacements. This evidence suggests that, under low-flow conditions, buoyancy becomes a significant factor. As the trajectory of the bubble demonstrates, its rise occurs after the frame corresponding to the initial phases of overtopping, thereby validating the efficacy of employing bubbles as tracers in our case. Caution should be exercised, however, when the flow speed significantly diminishes.

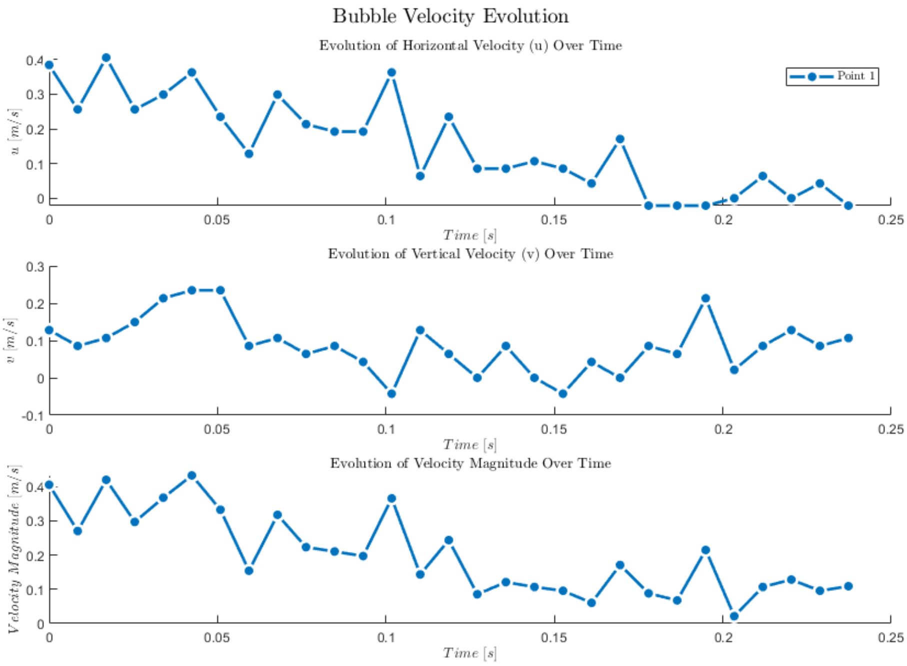

Figure 18: Evolution of the the velocity of the bubble, both in magnitude and for horizontal (u) and vertical (v) component.

3.3 Comparison with literature

The measured velocity has been compared with formulae from literature that allow the calculation of overtopping flow velocity at the dike. The maximum velocity measured at the seaward edge of a dike crest can be expressed as follows:

$$v_{max}(x_c = 0) = a_u\left(\sqrt{g(R_u - R_c)}\right)^{b_0} \tag{6}$$

With,

$$a_u = \begin{cases} 0.35\,cot\,\alpha\,,\ b_0 = 1.0 & (van\ der\ Meer\ et\ al., 2010) \\ 1.4, b_0 = 1.0 & (EurOtop\ ,2018) \\ 0.12\,cot\,\alpha + 0.41,\ b_0 = 1.35 & (Formentin\ et\ al., 2019) \end{cases} \tag{7}$$

Where R_c is the crest freeboard and R_u is the wave run-up height, being R_u- R_c the deficit in the freeboard as also described by Ibrahim and Baldock (2020). The aforementioned formulae encompass a range of dike slopes between 1:6 and 1:2, thus necessitating a judicious assessment of their applicability to steeper dikes. In the present case, the wave run-up height has been estimated on the basis of the formula proposed by Yuhi et al. (2020), which employs deep-water wave conditions. As the analysis considers the run-up associated with extreme events in an irregular sea state, the maximum wave run-up height has been employed, as defined below.:

$$(R_{max})_{99\%,100} = 1.54R_{u,2\%} \tag{8}$$

$$R_{u,2\%}/H_{mo,0} = 2.99 - 2.73exp\left(-0.57\ tan\beta \Big/ \sqrt{H_{mo,0}/L_o}\right) \tag{9}$$

Where L_o is the deep-water wave length. The slope β refers to the equivalent slope as defined in Yuhi et al. (2020). The calculated velocities ranged between 2 and 8 m/s, resulting in the Formentin et al. (2019) formula producing the lowest results, while the EurOtop (2018) formula yielded the highest. Measured velocities, scaled to prototype conditions, remain within the same order of magnitude, with the maximum value not exceeding 5.2 m/s.

4 Measurement uncertainties

Accurate measurement of overtopping flow velocities is critical for understanding and predicting coastal defence performance under extreme wave conditions. However, this task is fraught with several sources of uncertainty that can significantly impact the accuracy and reliability of the collected data. This section explores these uncertainties, focusing on key aspects such as the inherent variability of the overtopping process, the influence of three-dimensional (3D) effects and lighting conditions, and the complications arising from surface tension, scale/model effects, and bubble buoyancy in Bubble Image Velocimetry (BIV).

4.1 Overtopping process variability

Water-surface interaction processes, especially those characterized by significant turbulence, are subject to considerable variability (Marzeddu et al., 2017; Williams et al., 2019; Raby et al., 2022). In particular, the overtopping process is inherently variable. A minor fluctuation in factors such as wave height, period, and water level can result in a considerable discrepancy in overtopping discharges and volumes. This variability can result in significant fluctuations in flow velocity, which in turn complicates the measurement and interpretation of results. It is of paramount importance to gain an understanding of and to quantify this variability, as it has a significant impact on the reproducibility of experiments and the robustness of predictive models. The stochastic nature of wave overtopping necessitates the utilization of statistical methodologies that are capable of accurately capturing the range and distribution of potential flow velocities. In this study, a coefficient of variation between 1.8% and 6.6% was observed following the execution of 20 repetitions of the identical test case for each dike slope. It was found that steeper dikes and more turbulent and violent WSI resulted in elevated CoV values, indicating a reduction in repeatability.

4.2 3D effects & lighting

While many overtopping studies assume a two-dimensional (2D) flow field, in practice experiment might exhibit important 3D effects. These effects can arise from complex interactions between waves and structures, inaccuracies of the model building, etc., leading to spatial variations in flow velocity that are not captured in 2D analyses. Furthermore, the accuracy of optical measurement techniques, such as particle image velocimetry, is contingent upon the quality of the lighting conditions. Consequently, BIV is also affected by the lighting conditions. Inconsistent lighting can result in the formation of shadows and reflections that distort the perceived velocity field. Furthermore, some blurred areas presented in the background of the frames are elements that are not automatically excluded. Such factors can result in the acquisition of erroneous measurements. It is therefore essential to ensure careful calibration and control of lighting conditions in order to minimize these uncertainties (see also Formentin at al., 2024).

4.3 Scale and model effects

Surface tension and fluid viscosity is a significant factor, especially in small-scale model experiments, where the Weber and Reynolds number may differ substantially from that in real-life scenarios. The impact of surface tension can alter the flow characteristics, particularly in the presence of small-scale features such as bubbles and droplets. Scale/model effects further complicate the translation of laboratory findings to real-world applications, as the dynamic similarity between the model and the prototype may not be perfectly maintained. These effects must be accounted for to ensure that the experimental results are representative of full-scale conditions.

In this study, we conducted a preliminary assessment of scale effects by calculating the equivalent Reynolds and Weber numbers for wave overtopping and comparing them with thresholds proposed in the literature. Specifically, we verified that Req > 10^3 and Weq > 10, as suggested by Schüttrumpf and Oumeraci (2005).

Additionally, previous research has demonstrated that bubble fragmentation can be stabilized by surface tension at different scales, leading to varying levels of air entrainment (Miller, 1972; Deane and Stokes, 2002; Heller, 2011). This effect is scale-dependent and can significantly alter the dynamics of the overtopping flow. Recently, Na et al. (2018) concluded that the bubble size distribution does not hold at different scales, indicating the presence of scale effects. Furthermore, the content of air bubbles and bubble persistence differ between fresh and saltwater, affecting the characteristics of the overtopping flow. Seawater, with its higher salinity, increases surface tension, reducing bubble coalescence and promoting longer-lasting bubbles. Fresh water tends to contain fewer and larger bubbles compared to saltwater, which can influence the flow's behaviour and energy dissipation (Bullock et al., 2001). These differences might affect the accuracy of measurements using techniques like BIV, particularly in aerated flows, and should be considered when comparing results from different water types.

4.4 Buoyancy

The buoyancy of bubbles introduces additional uncertainties, as bubbles may rise or fall due to differences in density between the bubbles and the surrounding fluid. The effect of buoyancy can result in a distortion of the perceived velocity field, particularly in regions characterized by low flow velocities, where the influence of buoyancy is more pronounced. It is of the utmost importance to correct for these buoyancy effects in order to obtain accurate velocity measurements. In situations where significant bubble buoyancy is present, the measured bubble velocity, as determined by BIV, reflects the dynamics of the bubble itself. These dynamics are influenced by both the buoyant forces acting on the bubble and the movement of the surrounding fluid. The nature of this relationship is subject to variation depending on the direction and magnitude of the fluid velocity. For instance, in cases where the fluid velocity is small or negative, the buoyancy could cause the bubble velocity to appear greater than the surrounding fluid velocity. Consequently, the bubble's motion may appear counterintuitive, as the fluid flow may not always be in the same direction or magnitude as the bubble's trajectory. On the contrary, in the event of significant bubble buoyancy and positive fluid velocity directed upwards, the BIV will yield a bubble velocity that is greater than the fluid velocity (Ryu et al., 2005; Jayaratne et al., 2008; Raby et al., 2020). Therefore, careful interpretation is required when comparing bubble velocity measurements to the surrounding fluid's velocity in buoyant environments. It is critical to understand these nuances for correct interpretation of BIV measurements, especially when the flow conditions involve significant buoyancy effects. However, in the present study, buoyancy effects have been analysed (see Section 3.2.2), but not explicitly corrected. Whilst the results obtained might reflect the inherent buoyancy-driven deviations in velocity measurements, it is imperative to highlight these uncertainties in order to provide context and clarify the potential discrepancies in regions where buoyancy is more pronounced. Further research could involve the application of buoyancy corrections to refine the accuracy of velocity estimates obtained through BIV.

5 Discussions and Conclusions

The objective of this study was to demonstrate the applicability of BIV for measuring overtopping flow velocities in small wave flume experiments. The findings suggest that the methodology developed here can be extended to more typical coastal configurations and larger-scale experimental wave facilities, offering broader utility in coastal engineering research. The application of advanced measurement techniques, such as Bubble Image Velocimetry (BIV), has proven invaluable for detailed analyses of individual wave characteristics, essential for enhancing predictive models of wave overtopping. The research was conducted in a small-scale wave flume at the Marine Engineering Laboratory (LIM) of the Universitat Politècnica de Catalunya – BarcelonaTech (UPC). This controlled environment enabled the simulation of relevant wave conditions for coastal overtopping scenarios, utilizing BIV to capture and analyse the flow velocities associated with overtopping waves. This methodological approach provided high-resolution measurements and deep insights into the behaviour of individual waves, significantly advancing the field of coastal engineering.

BIV offers several advantages, including enhanced measurement capabilities that provide high temporal resolution, crucial for capturing the dynamics of overtopping flows. This capability allows for a better understanding of individual extreme waves, effectively visualizing and quantifying flow patterns and velocities that traditional methods might overlook. Moreover, as a non-intrusive technique, BIV does not interfere with the natural flow dynamics, preserving the integrity of the data collected. This non-intrusiveness is especially important in coastal engineering, where maintaining natural conditions is critical for accurate measurements. Additionally, BIV enables detailed characterization of flow velocities associated with individual waves, offering insights into the specific dynamics of overtopping events. Such detailed analysis is vital for developing more accurate predictive models for wave overtopping, crucial for designing and evaluating coastal defences.

The observation that the flow field during an overtopping event is non-uniform represents a particularly interesting result: one might initially hypothesise that the overtopping flow would exhibit a more uniform behaviour due to the relatively consistent physical conditions at the surface. However, the findings indicate substantial spatial and temporal variations in the flow velocity, which were effectively captured by the Bubble Image Velocimetry (BIV) technique. This non-uniformity calls into question the assumptions made by simplified models such as SWASH (a shallow water model commonly used for simulating wave-driven flows), which typically assume a more homogeneous flow structure. The BIV technique's capacity to elucidate these intricate flow patterns represents a substantial advantage, particularly in circumstances where conventional models may prove inadequate in capturing the subtleties of flow behaviour. This emphasises the necessity for sophisticated measurement techniques like BIV in accurately capturing the dynamics of overtopping flows, which can vary significantly over short distances and time scales.

The present study also recognises various uncertainties in measuring overtopping flow velocities, such as process variability and bubble buoyancy effects. Furthermore, the NewWave theory plays a pivotal role in this research by offering a framework for simulating extreme wave events in a realistic random sea state. This theory allows for modelling significant waves likely to cause overtopping, focusing on individual wave events rather than averaged characteristics. This focus is essential for understanding the specific dynamics and risks associated with overtopping waves, which can vary significantly in their impact on coastal structures. Yet, notwithstanding the demonstration in the study of the applicability and reproducibility of the BIV technique across a range of dike slopes, it is important to note the limitations of the technique when applied to a broader range of wave conditions. The use of a single focused wave group has been identified as a potential factor influencing the repeatability of the technique, and further investigation into this area is recommended.

Currently, the study focuses on a single moment within each test to present the results, which provides a snapshot of the flow conditions during the overtopping event. However, flow phenomena, especially in highly dynamic environments like overtopping events, are time-dependent. The flow velocity and structure can change rapidly, influenced by factors such as wave breaking, turbulence, and interaction with structures. A more detailed analysis of the time evolution of the flow field could yield valuable insights into the transient behaviours of the overtopping process. For instance, examining how the flow velocity evolves over time could help identify stages within the overtopping event where the flow is more chaotic or more uniform. Such an analysis might also reveal patterns or cycles within the overtopping process that could be critical for understanding the underlying physics. This could be the motivation of a future study, providing a more comprehensive understanding of the flow dynamics over time, potentially leading to improved predictive models. Future research should focus also on integrating advanced imaging techniques with hydrodynamic modelling to further refine predictions of wave overtopping. Besides, further research is needed to establish a more robust quantitative comparison with existing semi-empirical methods and data to fully assess the effectiveness of this technique. Future work should focus on systematically comparing experimental results with established literature and exploring the applicability of BIV in a broader range of coastal engineering scenarios. Additionally, developing standardized guidelines for assessing wave impacts on urban coastal infrastructure will be essential for mitigating the risks associated with extreme weather events and rising sea levels. This study lays a solid foundation for ongoing investigations into coastal safety and the complex dynamics of wave interactions with urban environments.

In conclusion, the application of BIV can be useful in providing detailed, accurate, and non-intrusive measurements of wave overtopping flows. These insights contribute to better predictive modelling and coastal management strategies, underlining the study's importance in enhancing infrastructure resilience and public safety in coastal areas. The research significantly advances the understanding of wave overtopping dynamics through the innovative use of BIV technique. The findings underscore the importance of precise measurements and detailed analyses in predicting wave behaviour and its impacts on coastal structures. These insights are crucial for refining predictive models, which can lead to improved safety measures and better management of coastal areas prone to flooding. The key findings of the research underscore the importance of analysing individual wave events. The integration of BIV with NewWave theory has led to the development of more precise predictive models, essential for the design and assessment of coastal defences.

Acknowledgements

The authors would like to express their gratitude to Joaquim Sospedra for his invaluable assistance during the experimental campaign.

Funding

This work was supported by the project GLORIA PID2020-115030RJ-I00 financed by MCIN/AEI/ 10.13039/501100011033 "Adquirir conocimientos sobre el riesgo de rebase para las zonas costeras urbanizadas". Besides, Dr. Corrado Altomare acknowledges funding from Spanish government and the European Social Found (ESF) under the programme ‘Ramón y Cajal 2020’ (RYC2020-030197-I / AEI / 10.13039/501100011033).

Author contributions (CRediT)

CA: Conceptualization, Data curation, Formal Analysis, Funding acquisition, Investigation, Methodology, Project administration, Resources, Software, Supervision, Validation, Visualization, Writing – original draft, Writing – review & editing.

XC: Data curation, Methodology, Software. Tomohiro Suzuki: Conceptualization, Investigation, Supervision, Writing – review & editing.

AR: Methodology, Supervision.

XG: Conceptualization, Investigation, Resources, Writing – review & editing.

Use of AI

During the preparation of this work the author(s) used DeepL Write in order to checking grammar, spelling. After using this tool/service, the author(s) reviewed and edited the content as needed and take(s) full responsibility for the content of the publication.

Data access statement

The data acquired in the study will be made available on request.

Declaration of interests

The author(s) report(s) no conflict of interest.

Notation

Name	Symbol	Unit
slope angle of dike	α	°
Linear focus amplitude	A	m
Coefficient for overtopping flow velocity calculation	a_u	-
Coefficient for overtopping flow velocity calculation	b_0	-
Equivalent slope	β	°
Circle of confusion	C	m
Depth of field	DoF	m
Focal length of the camera lens	f	m
Gravitational acceleration	g	m/s^2
Significant wave height of incident waves in deep waters, based on wave energy spectrum	$H_{m0,o}$	m
water depth (negative for emerged toe)	h	m
Overtopping layer thickness	h_A	m
Wavenumber of the i-th wave component	k_i	-

Deep-water wave length	L_0	m
wave length based on $T_{m-1,0}$ calculated using $L_{m-1,0} = (g/2\pi)\ T_{m-1,0}{}^2$	$L_{m-1,0}$	m
Infinitesimal wave component	N	-
distance for the focal plane	L	m
F-number of the camera aperture	n	-
Nearest limit of depth of field	R	m
Freeboard (crest height relative to still water level)	R_c	m
Equivalent Reynolds number	$Re_q = \frac{2(R_u - R_c)^2}{\nu_w T}$	-
Wave run-up height	R_u	m
The average runup of the highest 2% of waves	$R_{u,2\%}$	m
Maximum wave run-up height	$R_{max99\%,100}$	m
Farthest limit of depth of field	S	m
Power spectral density	$S_{\eta\eta}$	m^2/Hz
Time	t	s
Focus time	t_f	s
Mean period	T	s
Peak period	T_p	s
Flow velocity	v	m/s
Maximum velocity at the seaward edge of the dike crest ($x_c = 0$)	v_{max}	m/s
Equivalent Weber number	$We_q = \frac{v h_A \rho_w}{\sigma_w}$	-
Horizontal distance from wave generation	x	m
Location at the dike crest from wave generation	x_c	m
Focus location from wave generation	x_f	m
Water surface elevation	$\eta(x,t)$	m
Water kinematic viscosity	ν_w	m^2/s
Water density	ρ_w	kg/m^3
Phase angle of the group at focus	ϕ	°
Mean of the calculated velocities of repeated tests	μ	m/s
Angular frequency	ω	rad/s
Angular frequency of the i-th wave component	ω_i	rad/s
Standard deviation of the sea state	σ	m
Standard deviation of the calculated velocities of repeated tests	σ'	m/s
Variance of the sea state	σ^2	m^2
Water surface tension	σ_w	N/m

Abbreviations

AWG0	Ultrasonic proximity sensor at 9.58 m from the wave generator
AWG1	Ultrasonic proximity sensor in the overtopping tank
BIV	Bubble Image Velocimetry
CCC	Concordance Correlation Coefficient
CIEMito	Small-scale wave flume at Universitat Politècnica de Catalunya - BarcelonaTech
DOF	Depth of Field
LIM	Maritime Engineering Laboratory
Lmf	Local median filter
MAE	Mean Absolute Error
PIV	Particle Image velocimetry
R^2	Robust Coefficient of Determination
ROI	Region of Interest
Stdf	Standard deviation filter
VDP	Valid detection probability
WG0-WG7	Resistive wave gauges
WSI	Wave structure interaction

References

Altomare, C., Gironella, X., Suzuki, T., Viccione, G., Saponieri, A. (2020). Overtopping Metrics and Coastal Safety: A Case of Study from the Catalan Coast. *J. Mar. Sci. Eng.*, 8, 556. https://doi.org/10.3390/jmse8080556.

Bae, Hyun-Ung, Yun, K.M., Yoon, J.Y. and Lim, N.H. (2016). Human stability with respect to overtopping flow on the breakwater. *Int. J. Appl. Eng. Res*. 2016, 11, 111–119.

Arrighi, C., Oumeraci, H. and Castelli, F. (2017). Hydrodynamics of pedestrians' instability in floodwaters. *Hydrol. Earth Syst. Sci.*, 21, 515–531, https://doi.org/10.5194/hess-21-515-2017.

Bullock, G.N., Crawford, A.R., Hewson, P.J., Walkden, M.J.A., Bird, P.A.D. (2001). The influence of air and scale on wave impact pressures. *Coastal Engineering*, Volume 42, Issue 4, https://doi.org/10.1016/S0378-3839(00)00065-X.

Chuang, W.-L. (2024). On the fluid kinematics of common types of greenwater events: An experimental study. *Applied Ocean Research*, Volume 153, https://doi.org/10.1016/j.apor.2024.104235.

Deane, G., Stokes, M. (2002). Scale dependence of bubble creation mechanisms in breaking waves. *Nature*, 418, 839–844. https://doi.org/10.1038/nature00967.

Endoh, K., Takahashi, S. (1995) Numerically modelling personnel danger on a promenade breakwater due to overtopping waves. *24th International Conference on Coastal Engineering*. https://doi.org/10.1061/9780784400890.075.

EurOtop. (2018) Manual on wave overtopping of sea defences and related structures. An overtopping manual largely based on European research, but for worldwide application. Van der Meer, J.W., Allsop, N.W.H., Bruce, T., De Rouck, J., Kortenhaus, A., Pullen, T., Schüttrumpf. [Online]. Available: www.overtopping-manual.com

Formentin, S.M., Gaeta, M.G., Palma, G, Zanuttigh, B., Guerrero, M. (2019). Flow Depths and Velocities across a Smooth Dike Crest. *Water*, 11, 2197; https://doi.org/10.3390/w11102197.

Formentin, S.M., Altomare, C., Marzeddu, A., Zanuttigh, B. (2024). Image clustering for overtopping volume measurements. *Physics of Fluids*, 36 (6): 065137. https://doi.org/10.1063/5.0207486.

Garzon, J.L., Ferreira, Ó., Reis, M.T. et al. (2023). Conceptual and quantitative categorization of wave-induced flooding impacts for pedestrians and assets in urban beaches. *Sci Rep 13*, 7251. https://doi.org/10.1038/s41598-023-32175-6.

Greco, M., Colicchio, G., Faltinsen, O.M., 2007. Shipping of water on a two-dimensional structure. Part 2. *J. Fluid. Mech*. 581, 371–399, https://doi.org/10.1017/S002211200700568X.

Heller, V. (2011). Scale effects in physical hydraulic engineering models. *Journal of Hydraulic Research*, vol. 49, no. 3, pp. 293–306, https://doi.org/10.1080/00221686.2011.578914.

Hofland, B., Wenneker, I., Van Steeg, P. (2014) Short test durations for wave overtopping experiments. *Proceedings of the 5th International Conference on the Application of Physical Modelling to Port and Coastal Protection*, Varna, Bulgaria (2014), pp. 349-358A.C.

Huber, P. J. (1964). Robust Estimation of a Location Parameter. *The Annals of Mathematical Statistics*, 35(1), 73-101.

Hughes, S.A. and Thornton, C.I. (2016). Estimation of time-varying discharge and cumulative volume in individual overtopping waves. *Coastal Engineering*, vol. 117, pp. 191–204, https://doi.org/10.1016/j.coastaleng.2016.08.006.

Ibrahim, M.S.I. and Baldock, T.E. (2020). Swash overtopping on plane beaches – Reconciling empirical and theoretical scaling laws using the volume flux. *Coastal Engineering*, vol. 157, p. 103668, doi: https://doi.org/10.1016/j.coastaleng.2020.103668.

Koosheh, A., Etemad-Shahidi, A., Cartwright, N., Tomlinson, R., Van Gent, M.R.A. (2021). Individual wave overtopping at coastal structures: A critical review and the existing challenges. *Applied Ocean Research*, vol. 106, p. 102476, https://doi.org/10.1016/j.apor.2020.102476.

Jayaratne, R., Raby, A., Bullock, G., Henrik, B. (2009). Individual violent overtopping events: New insights. *Proceedings of the Coastal Engineering Conference*. 2983-2995. https://doi.org/10.1142/9789814277426_0247.

Lee, G.N., Jung, K.H., Shin, S.Y., Park, H.J., Malenica, S., Chung, Y. S., Suh, S.B (2022). Experimental study of green water on rectangular structure with varying flare angle. *Ocean Engineering*, Volume 243, https://doi.org/10.1016/j.oceaneng.2021.110252.

Lin L. I. (1989). A concordance correlation coefficient to evaluate reproducibility. *Biometrics*, 45(1), 255-268.

Mares-Nasarre, P., Argente, G., Gómez-Martín, M.E., Medina, J.R. (2019). Overtopping layer thickness and overtopping flow velocity on mound breakwaters, *Coastal Engineering*, Volume 154, https://doi.org/10.1016/j.coastaleng.2019.103561.

Marzeddu, A., Oliveira, T.C.A., Gironella, X., Sánchez-Arcilla, A. (2017). Variability of wave impact measurements on vertical breakwaters. *Journal of Hydraulic Research*, 55:6, 772-786. https://doi.org/10.1080/00221686.2017.1312576.

Miller, R. (1972). The role of surface tension in breaking waves. *Coastal Engineering*, https://doi.org/10.1061/9780872620490.025

Na, B, Chang, K.-A., Huang, Z.-C., Hsu, W.-I., Chuang, W.-L., Chen, Y.-Y (2018). Large-scale laboratory observation of flow properties in plunging breaking waves. *Coastal Engineering*, Volume 138, pages 66-79, https://doi.org/10.1016/j.coastaleng.2018.04.002.

Raby, A., Jayaratne, R., Bredmose, H., & Bullock, G. (2019). Individual violent wave-overtopping events: behaviour and estimation. *Journal of Hydraulic Research*, *58*(1), 34–46. https://doi.org/10.1080/00221686.2018.1555549.

Raby, A., Jayaratne, R., Bredmose, H., Bullock, G. (2020). Individual violent wave-overtopping events: behaviour and estimation. Journal of Hydraulic Research, 58:1, 34-46, https://doi.org/10.1080/00221686.2018.1555549.

Raby, A., Bullock, G., Jonathan, P., Randell, D., Whittaker, C. (2022). On wave impact pressure variability. *Coastal Engineering*, Volume 177. https://doi.org/10.1016/j.coastaleng.2022.104168

Renaud, O., Victoria-Feser, M.-P. (2010). A robust coefficient of determination for regression. *Journal of Statistical Planning and Inference*, Volume 140, Issue 7, https://doi.org/10.1016/j.jspi.2010.01.008.

Rivillas-Ospina, G., Pedrozo-Acuña, A., Silva, R., Torres-Freyermuth, A., Gutierrez C. (2012) Estimation of the velocity field induced by plunging breakers in the surf and swash zones. *Experiments in Fluids*. 52. 53-68. https://doi.org/10.1007/s00348-011-1208-x.

Ryu, Y., Chang, K.A., Lim, H.J. (2005). Use of bubble image velocimetry for measurement of plunging wave impinging on structure and associated greenwater. *Measurement Science and Technology* 16, 1945–1953. https://iopscience.iop.org/article/10.1088/0957-0233/16/10/009.

Sandoval, C, Bruce, T. (2017) Wave overtopping hazard to pedestrians: video evidence from real accidents. Coasts, Marine Structures and Breakwaters 2017, Liverpool, UK: ICE Publishing, 2018, pp. 501–512. doi: https://doi.org/10.1680/cmsb.63174.0501.

Schüttrumpf, H. (2001). Wellenüberlaufströmung bei Seedeichen – Experimentelle und Theoretische Untersuchungen. PHD-Thesis. http://www.biblio.tu-bs.de/ediss/data/20010703a/20010703a.html

Schüttrumpf, O. and Oumeraci, H. (2005) Layer thicknesses and velocities of wave overtopping flow at seadikes. *Coastal Engineering*, vol. 52, no. 6, pp. 473–495, https://doi.org/10.1016/j.coastaleng.2005.02.002.

Stokes, K., Poate, T., Masselink, G., King, E., Saulter, A., Ely, N. (2021) Forecasting coastal overtopping at engineered and naturally defended coastlines. *Coastal Engineering*, Volume 164. https://doi.org/10.1016/j.coastaleng.2020.103827.

Thielicke, W., Sonntag, R. (2021). Particle Image Velocimetry for MATLAB: Accuracy and enhanced algorithms in PIVlab. *Journal of Open Research Software*, 9(1): p.12. http://doi.org/10.5334/jors.334.

Thielicke, W. & Stamhuis, E.J. (2014). PIVlab – Towards User-friendly, Affordable and Accurate Digital Particle Image Velocimetry in MATLAB. *Journal of Open Research Software*, 2(1):e30. http://dx.doi.org/10.5334/jors.bl.

Tromans, P.S., Anaturk, A.R., Hagemeijer, P. (1991) A new model for the kinematics of large ocean waves - application as a design wave. *Proceedings of the First International Offshore and Polar Engineering Conference*, The International Society of Offshore and Polar Engineers, pp. 64-71.

Van Bergeijk, V.M., Warmink, J.J., van Gent, M.R.A., Hulscher, S.J.M.H. (2019). An analytical model of wave overtopping flow velocities on dike crests and landward slopes. *Coastal Engineering*. https://doi.org/10.1016/j.coastaleng.2019.03.001.

Van der Meer, J., Steendam, G. J., Bruce, T. & Klein, Breteler M. (2022) Admissible post-wave overtopping flow for persons on a horizontal surface. *Journal of Coastal and Hydraulic Structures*, 2, p.15. https://doi.org/10.48438/jchs.2022.0015.

Westerweel, J., Scarano, F. (2005). Universal outlier detection for PIV data. *Exp Fluids* 39, 1096–1100. https://doi.org/10.1007/s00348-005-0016-6.

Whittaker, C.N., Fitzgerald, C.J., Raby, A.C., Taylor, P.H. (2016) The average shape of large waves in the coastal zone. *Coastal Engineering*, vol. 114, pp. 253–264. https://doi.org/10.1016/j.coastaleng.2016.04.009.

Whittaker, C.N., Fitzgerald, C.J., Raby, A.C., Taylor, P.H., Orszaghova, J. and Borthwick, A.G.L. (2017) Optimisation of focused wave group runup on a plane beach. *Coastal Engineering*, vol. 121, pp. 44–55. doi: https://doi.org/10.1016/j.coastaleng.2016.12.001.

Whittaker, C.N., Fitzgerald, C.J., Raby, A.C., Taylor, P.H, and Borthwick, A.G.L. (2018) Extreme coastal responses using focused wave groups: Overtopping and horizontal forces exerted on an inclined seawall. *Coastal Engineering*, vol. 140, pp. 292–305. https://doi.org/10.1016/j.coastaleng.2018.08.004.

Williams, H.E., Briganti, R., Romano, A., Dodd, N. (2019). Experimental Analysis of Wave Overtopping: A New Small Scale Laboratory Dataset for the Assessment of Uncertainty for Smooth Sloped and Vertical Coastal Structures. *J. Mar. Sci. Eng.* 7, 217. https://doi.org/10.3390/jmse7070217.

Yuhi, M., Mase, H., Kim, S., Umeda, S. and Altomare, C. (2020) Refinement of integrated formula of wave overtopping and runup modeling. *Ocean Engineering*, 2021, vol. 220, p. 108350. https://doi.org/10.1016/j.oceaneng.2020.108350.